Inorganic Chemistry

Article

pubs.acs.org/IC

# Solvent-Mediated Crystal-to-Crystal Interconversion between Discrete Lanthanide Complexes and One-Dimensional Coordination Polymers and Selective Sensing for Small Molecules

Jin-Ji Wu,[†] Yu-Xin Ye,[†] Ying-Yu Qiu,[†] Zheng-Ping Qiao,[†] Man-Li Cao,*[,‡] and Bao-Hui Ye*[,†]

[†]MOE Key Laboratory of Bioinorganic and Synthetic Chemistry, School of Chemistry and Chemical Engineering, Sun Yat-Sen University, Guangzhou 510275, China

[‡]Department of Chemistry, Guangdong University of Education, Guangzhou 510303, China

Supporting Information

**ABSTRACT:** Two isostructural 1D coordination polymers $\{[Ln(OAc)_2(H_2O)(OBPT)]\cdot 3H_2O\}_n$ (HOBPT = 4,6-bis(2-pyridyl)-1,3,5-triazin-2-ol, Ln = $Eu^{3+}$, **1**; $Tb^{3+}$, **3**) and two discrete complexes $[Ln(OAc)_2(DMF)_2(OBPT)]$ (Ln = $Eu^{3+}$, **2**; $Tb^{3+}$, **4**) have been synthesized in $H_2O$−MeOH or DMF solvents, respectively. Their structures were identified by powder X-ray diffraction. Single-crystal X-ray studies for complexes **1** and **2** revealed that the coordination geometries of the $Eu^{3+}$ ions are similar and can be described as a distorted tricapped trigonal prism with six oxygen atoms and three nitrogen atoms. The difference between them is that one aqua ligand and one oxygen atom from the OBPT ligand complete the coordination sphere in complex **1**, whereas two DMF molecules complete the coordination sphere in complex **2**. Interestingly, the solvent-mediated, reversible crystal-to-crystal transformation between them was achieved by immersing the crystalline samples in the corresponding solvent ($H_2O$ or DMF) or by exposing them to solvent vapor. Complex **1** shows a highly selective luminescence enhancement in response to DMF in comparison to that observed in response to other examined solvents such as acetone, ethyl acetate, ethanol, acetonitrile, methanol, and THF.

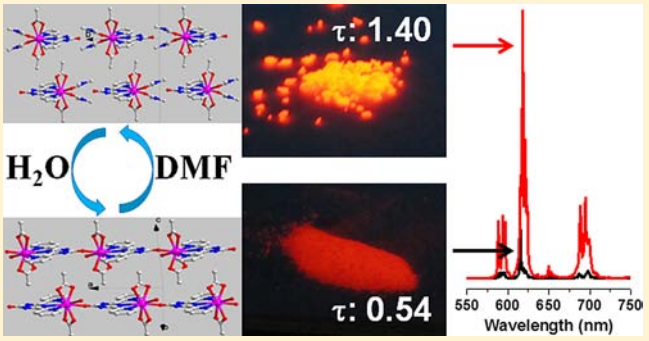


## INTRODUCTION

Crystal-to-crystal (including single-crystal−single-crystal) transformation has received considerable attention in solid-state reactions for crystal engineering.[1,2] It provides opportunities to understand solid-state transformations and to prepare new functional materials under external stimuli such as thermal,[3] photo,[4] solvent molecules,[5] mechanical forces,[6] and anions or cations.[7] Although high-dimensional coordination polymers with a high stability and porous crystallinity have been widely observed in reversible crystal-to-crystal transformations,[2,8] the cases of conversion between discrete complexes and high-dimensional coordination polymers are still rare.[9] Unlike the simple guest exchange or absorption/desorption, these conversions involve bond formation and breakage, leading to the loss of crystallinity and changes in physical properties such as color,[9d,g,i] magnetism,[9b,j,k,m] luminescence,[10] chirality,[9h] and absorption.[9l] Generally, the existence of an uncoordinated atom that is close to the metal ion is necessary for this conversion to occur.[2d]

Our previous work has shown that ligand 4,6-bis(2-pyridyl)-1,3,5-triazin-2-ol (HOBPT) is a multidentate ligand that has various coordination modes (Scheme 1). In some cases the oxygen and/or nitrogen atoms are uncoordinated. Using this ligand, a nanocage cation $[Co(H_2O)_6\subset Co_8(OBPT)_{12}]^{6+}$ has been successfully assembled in the presence of a $Co^{2+}$ ion with a cis−cis bis-bidentate mode.[11] When a $Cu^{2+}$ ion was introduced, mononuclear,[12] tetra-nuclear,[13] and eighteen-nuclear[14] complexes as well as a zigzag chain polymer[13] were obtained. In these cases, the oxygen atom is either uncoordinated or weakly coordinated to the $Cu^{2+}$ ion. Interestingly, when hard-metal ions such as $Na^+$, $Ca^{2+}$, and $Ba^{2+}$ are present, 1D coordination polymers in which the oxygen atom further bound to the metal ion were obtained,[15] resulting in a mono/tridentate coordination mode. As part of an ongoing study, we have extended the observation of the reaction of the ligand toward rare-earth ions in various solvents. Delightedly, two isostructural 1D coordination polymers $\{[Ln(OAc)_2(H_2O)(OBPT)]\cdot 3H_2O\}_n$ (Ln = $Eu^{3+}$, **1**; $Tb^{3+}$, **3**) and two discrete complexes $[Ln(OAc)_2(DMF)_2(OBPT)]$ (Ln = $Eu^{3+}$, **2**; $Tb^{3+}$, **4**) were afforded from the $H_2O$−MeOH and DMF solvents, respectively. Furthermore, crystal-to-crystal interconversions between the 1D coordination polymers and the discrete complexes were achieved. Their luminescence

**Received:** February 9, 2013
**Published:** May 22, 2013

   dx.doi.org/10.1021/ic400340y | Inorg. Chem. 2013, 52, 6450−6456

**Scheme 1. Various Coordination Modes for the HOBPT Ligand**

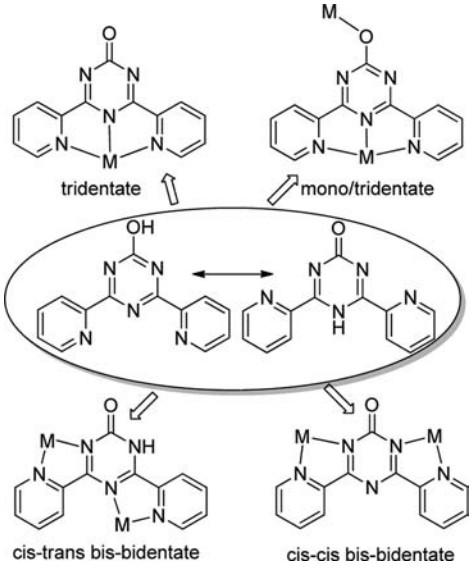


properties were also observed. Complex **1** shows a highly selective luminescence enhancement in response to DMF in comparison to that observed in response to other examined solvents, indicating that it is a potential sensing material for DMF.

## EXPERIMENTAL SECTION

**Materials and Methods.** The reagents and solvents were commercially available and used as received without further purification except for the solvents that were used in the luminescence experiments, which were dried with 4 A molecular sieves. $\{[Na(OBPT)(H_2O)]\cdot 2H_2O\}_n$ was prepared according to a previously reported procedure.[15] The C, H, and N microanalyses were carried out with a Vario EL elemental analyzer. The FTIR spectra were recorded from KBr pellets in the range of 400−4000 $cm^{-1}$ on a Bruker Tensor 27 spectrometer. The thermogravimetric data were collected on a Netzsch TGS-2 analyzer under a nitrogen atmosphere at a heating rate of 10 °C $min^{-1}$. The powder X-ray diffraction (PXRD) patterns were recorded on a D/Max-2200 diffractometer with Cu K$\alpha$ radiation ($\lambda$ = 1.5409 Å) at a scanning rate of 4° $min^{-1}$ with 2$\theta$ ranging from 5 to 35°. Samples that were used for luminescence measurements were checked by PXRD to ensure that they were in the pure phase. The photoluminescence spectra were recorded on an Edinburgh Instruments, Ltd. spectrometer (FLSP920). All instrument parameters, such as the incident and emergent slit widths (0.2 mm for the incident and emergent slits) and scanning speed (dwell time, 0.5 s; step, 0.5 nm), were fixed for all measurements, and all samples were loaded as soon as possible and sealed in small quartz cells for measurements.

**Synthesis of $\{[Ln(OAc)_2(H_2O)(OBPT)]\cdot 3H_2O\}_n$ (Ln = Eu, 1; Tb, 3).** $Ln(OAc)_3\cdot H_2O$ (400 mg, 1 mmol) and $\{[Na(OBPT)(H_2O)]\cdot 2H_2O\}_n$ (327 mg, 1 mmol) were dissolved in 20 mL of $H_2O$−MeOH (1:1), and the clear solution was stirred at room temperature for 2 h. The resulting white crystallites were filtered, washed with 5 mL of distilled water, and air dried. For complex **1**, the yield was 96%. Anal. Calcd for $C_{17}H_{22}EuN_5O_9$: C, 34.47; H, 3.74; N, 11.82. Found: C, 34.76; H, 3.86; N, 11.76. FTIR (KBr, $cm^{-1}$): 3402 (w), 1543 (vs), 1472 (s), 1433 (m), 1379 (m), 1300 (w), 1258 (w), 1057 (w), 1014 (w), 804 (w), 760 (w), 679 (w), 636 (w). Single crystals of complex **1** that were suitable for X-ray structure determination were carefully grown by diffusing the NaOBPT solution into the solution containing $Eu(OAc)_3$ for 2 weeks. The pure phase of the as-synthesized powdery solid was examined by PXRD (Figure S1 in the Supporting Information).

For complex **3**, the yield was 95%. Anal. Calcd for $C_{17}H_{22}TbN_5O_9$: C, 34.07; H, 3.70; N, 11.69. Found: C, 33.80; H, 3.89; N, 11.44. FTIR (KBr, $cm^{-1}$): 3386 (w), 1543 (vs), 1473 (s), 1435 (m), 1381 (m), 1300 (w), 1256 (w), 1055 (w), 1014 (w), 800 (w), 758 (w), 679 (w), 634 (w).

**Synthesis of $[Ln(OAc)_2(DMF)_2(OBPT)]$ (Ln = Eu, 2; Tb, 4).** $Ln(OAc)_3\cdot H_2O$ (400 mg, 1 mmol) and $\{[Na(OBPT)(H_2O)]\cdot 2H_2O\}_n$ (327 mg, 1 mmol) were dissolved in 10 mL of dried DMF, and the clear solution was stirred at room temperature for 2 h. The resulting white powdery solid was filtered, washed with 5 mL of DMF, and dried in a desiccator. For complex **2**, the yield was 65%. Anal. Calcd for $C_{23}H_{28}EuN_7O_7$ (**2**): C, 41.45; H, 4.23; N, 14.71. Found: C, 41.84; H, 4.56; N, 14.45. FTIR (KBr, $cm^{-1}$): 3082 (w), 2983 (w), 2939 (w), 1658 (vs), 1614 (s), 1544 (vs), 1421 (vs), 1384 (s), 1294 (m), 1253 (m), 1111 (w), 1049 (w), 1010 (m), 929 (w), 808 (m), 763 (m), 715 (w), 673 (m), 636 (w), 617 (w), 478 (w), 414 (m). Single crystals suitable for the X-ray structure determination of complex **2** were carefully grown by diffusing the NaOBPT DMF solution into the DMF solution containing $Eu(OAc)_3$ for 3 months. The pure phase of the as-synthesized powdery solid was examined by PXRD (Figure S2 in the Supporting Information).

For complex **4**, the yield was 73%. Anal. Calcd for $C_{23}H_{28}TbN_7O_7$: C, 41.02; H, 4.19; N, 14.56. Found: C, 40.85; H, 4.42; N, 14.31. FTIR (KBr, $cm^{-1}$): 3081 (w), 2983 (w), 2939 (w), 1657 (vs), 1615 (s), 1544 (vs), 1421 (vs), 1385 (s), 1294 (m), 1253 (m), 1112 (w), 1050 (w), 1010 (m), 929 (w), 807 (m), 763 (m), 715 (w), 673 (m), 636 (w), 617 (w), 479 (w), 414 (m).

**Single-Crystal X-ray Crystallography.** The diffraction intensities for **1** and **2** were collected at 123 K on a Bruker Smart Apex CCD diffractometer with graphite-monochromated Mo K$\alpha$ radiation ($\lambda$ = 0.71073 Å). Absorption corrections were applied using SADABS.[16] The structures were solved by direct methods and refined with full-matrix least-squares techniques using the SHELXS-97 and SHELXL-97 programs, respectively.[17,18] Anisotropic thermal parameters were applied to all nonhydrogen atoms. The organic hydrogen atoms were generated geometrically. The hydrogen atoms of the water molecules were located from difference maps and refined with isotropic temperature factors. The crystal data and the details of the data collection and refinement for the complexes are summarized in Table 1. Selected bond distances and angles are listed in Table S1 in the Supporting Information.

**Crystal-to-Crystal Transformations.** The microcrystalline samples of complexes **1** and **3** (30 mg) were immersed in screw-capped vials with 1 mL of DMF for 20 and 40 min, respectively. The DMF

**Table 1. Crystal Data and Structure Refinement for 1 and 2**

| complex | **1** | **2** |
|---|---|---|
| molecular formula | $C_{17}H_{22}EuN_5O_9$ | $C_{23}H_{28}EuN_7O_7$ |
| $M_r$ | 592.36 | 666.48 |
| crystal system | triclinic | monoclinic |
| space group | $P\bar{1}$ | $C2/c$ |
| $a$ (Å) | 8.4942(5) | 16.4951(9) |
| $b$ (Å) | 9.8122(6) | 12.0236(6) |
| $c$ (Å) | 12.9285(8) | 15.6395(8) |
| $\alpha$ (deg) | 81.7788(10) | 90 |
| $\beta$ (deg) | 85.1860(10) | 120.7840(10) |
| $\gamma$ (deg) | 87.5320(10) | 90 |
| $V$ (Å$^3$) | 1062.18(11) | 2664.8(2) |
| $Z$ | 2 | 4 |
| $D_c$ (g $cm^{-3}$) | 1.852 | 1.661 |
| $\mu$ ($mm^{-1}$) | 3.013 | 2.409 |
| data/restraints/parameters | 3622/0/289 | 2616/0/174 |
| R1 [$I > 2\sigma(I)$]$^a$, wR2$^b$ (all data) | 0.0221, 0.0599 | 0.0203, 0.0537 |
| GOF on $F^2$ | 1.162 | 1.087 |
| $\Delta\rho_{max}/\Delta\rho_{min}$(e Å$^{-3}$) | 1.44/−0.50 | 0.71/−0.55 |

$^a$R1 = $\sum||F_o| - |F_c||/\sum|F_o|$, $^b$wR2 = $[\sum w(F_o^2 - F_c^2)^2/\sum w(F_o^2)^2]^{1/2}$


dx.doi.org/10.1021/ic400340y | Inorg. Chem. 2013, 52, 6450−6456

solvent was removed with a dropper, and the solvent on the surface of the samples was absorbed with filter paper and dried. Microcrystalline samples of complexes **2** and **4** were placed on a specimen glass and drenched with a few drops of water. The samples were absorbed with filter paper and dried as soon as possible. For solid−gas transformations, microcrystalline samples of **1** or **2** were exposed to DMF vapor for 3 weeks or water vapor for 1 day at room temperature. The single-crystal−single-crystal transformations were also examined in our samples; however, the resulting crystals were unsuitable for single-crystal X-ray diffraction. Therefore, PXRD was used to confirm the phase transformation.

## RESULTS AND DISCUSSION

**Synthesis and Characterization.** Our previous work has shown that HOBPT is a mutlidentate ligand with various coordination modes.[11−15] Among them, the tetradentate mode of the sodium, calcium, and barium complexes attracted our attention. After taking the coordinate behavior of rare-earth ions into consideration, we used luminescent $Eu^{3+}$ and $Tb^{3+}$ ions to synthesize 1D coordination polymers that are analogous to that of the calcium complex.[15] As expected, two coordination polymers, **1** and **3**, were obtained by reacting equivalent amounts of ligand with $Eu(OAc)_3$ or $Tb(OAc)_3$ in a $H_2O$−MeOH solution. The reaction was almost complete in 2 h with high yields of 96% for complex **1** and 95% for complex **3**. The structure of complex **1** was measured by single-crystal X-ray diffraction. However, the single crystals of **3** were too small to measure by X-ray diffraction, even though we have made many attempts to do so. Fortunately, the PXRD patterns of the as-synthesized products of **1** and **3** were closely matched to the simulated pattern from the single-crystal data of **1** (Figure S1 in the Supporting Information), indicating that complexes **1** and **3** are isomorphous. Surprisingly, when the reactions were carried out in DMF, complexes **2** and **4** were afforded in moderate yields of 65−75%. However, their crystal phase changed from triclinic to monoclinic. Single-crystal measurement of complex **2** revealed that it is a discrete complex in which two DMF molecules occupy the coordination sphere of the $Eu^{3+}$ ion, as opposed to the oxygen atoms from the OBPT ligand and the $H_2O$ molecule in **1**. The identical phase of **2** and **4** was also examined by PXRD (Figure S2 in the Supporting Information), indicating that they are isomorphous. It is worth noting that complexes **2** and **4** were not isolated from the undried DMF solution in our experiments.

Furthermore, thermal gravimetric analysis (TGA) was performed to examine the water molecules in complexes **1** and **3**. For complex **1**, the weight loss of 9.4% in the range of 25−90 °C corresponds to the loss of three lattice water molecules (cal. 9.1%, Figure S3 in the Supporting Information). By increasing the temperature, the weight loss of 3.1% in the range of 90−150 °C should correspond to the loss of the one coordinated water molecule (cal. 3.1%). Beyond this range, there is a plateau that extends to approximatly 320 °C. For complex **3**, the TGA curve is very similar to that of **1**. The curve indicates the elimination of three lattice water molecules (9.0%, cal. 9.1%) and one coordination water molecule (3.2%, cal. 3.1%) in the ranges of 25−88 °C and 88−150 °C, respectively (Figure S4 in the Supporting Information).

**Crystal Structures of Complexes 1 and 2.** Single-crystal X-ray diffraction analysis revealed that complex **1** crystallizes in the $P\bar{1}$ space group. The asymmetric unit of **1** contains one $[Eu(OAc)_2(H_2O)(OBPT)]$ molecule and three water molecules. As shown in Figure 1, each $Eu^{3+}$ ion is nine-coordinated by four oxygen atoms from two acetates (Eu−O = 2.41−2.50 Å) and three nitrogen atoms from one OBPT ligand (Eu−N = 2.539(3) and 2.583(3) Å) as well as one aqua (Eu−O = 2.441(2) Å) and one oxygen atom from the neighboring OBPT (Eu−O = 2.363(2) Å). The coordination geometry of the $Eu^{3+}$ center can be described as a distorted tricapped trigonal prism. Along the *a* axis, the OBPT ligands connect the $[Eu(OAc)_2(H_2O)]^+$ units into a 1D coordination polymer in a head-to-tail fashion (Figure 2). The chain is further stabilized

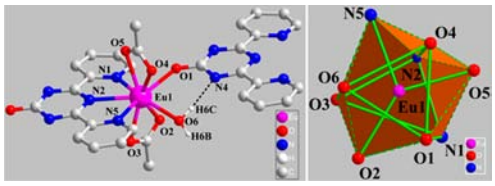


**Figure 1.** View of the coordination geometry (left) and polyhedron (right) of the $Eu^{3+}$ ion in complex **1**.

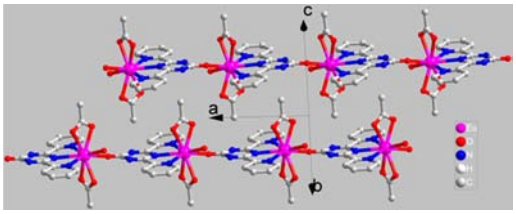


**Figure 2.** View of two coordination polymer chains in complex **1** along the *a* axis. The hydrogen atoms are omitted for clarity.

by the hydrogen bonds of the aqua and the uncoordinated nitrogen atom of the OBPT ligand (O6···N4 = 2.843(4) Å) (Figure 1). The Lattice water molecules are packed among the chains.

Complex **2** crystallizes in the *C*2/*c* space group. Similar to complex **1**, the $Eu^{3+}$ ion is nine-coordinated with a distorted tricapped trigonal prism geometry. However, two DMF molecules are coordinated to the $Eu^{3+}$ ion (Eu−O = 2.411(1) Å), as opposed to the aqua and oxygen atoms of OBPT in complex **1**, resulting in a discrete complex (Figures 2 and 3). Along the Eu−N2 bond, a $C_2$ axis is observed in the

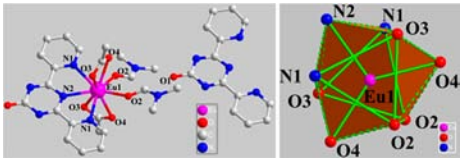


**Figure 3.** View of the coordination geometry (left) and polyhedron (right) of the $Eu^{3+}$ ion in complex **2**. Symmetry code: *a*, $-x + 1$, $y$, $-z + {}^3/_2$.

coordination sphere in complex **2**. Although the oxygen atom from OBPT ligand is uncoordinated to the $Eu^{3+}$ ion, it forms hydrogen bonds with the two DMF molecules (O1···C10 = 3.20, H10A···O1 = 2.47, O1···C12 = 3.27, and H12A···O1 = 2.49 Å), resulting in a 1D hydrogen-bonded chain along the *b* axis (Figure 4). In this regard, its head-to-tail assembly looks similar to that of complex **1**. The uncoordinated oxygen is near $Eu^{3+}$ (Eu···O = 5.484(2) Å). Upon comparison of the crystal structure of **1** and **2**, we speculated that they may be good candidates for examining crystal-to-crystal transformation by the exchange of coordination atoms, leading to a coordination


dx.doi.org/10.1021/ic400340y | Inorg. Chem. 2013, 52, 6450−6456

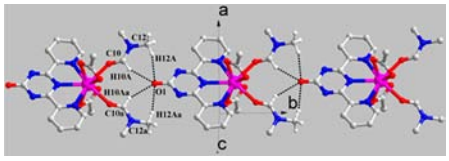


**Figure 4.** View of the packing of complex **2** along the *b* axis. The hydrogen atoms are omitted for clarity. Symmetry code: *a*, $-x + 1$, *y*, $-z + {}^{3}/_{2}$.

geometry rearrangement due to the hard and O-favored rare-earth ion.

**Crystal-to-Crystal Transformation.** Generally, the removal of coordinated molecules leads to a structural rearrangement in the coordination sphere. In these cases, the weakly coordinated molecule (i.e., the solvents) may be lost under external stimuli, leading to the creation of a vacant coordination site whereby the uncoordinated atoms of the already-attached ligand closest to the metal center may move and bind to the metal ion.[2d] In complex **2**, two DMF molecules bind to the $Eu^{3+}$ ion in a monodentate mode, and the uncoordinated oxygen atoms are close to the $Eu^{3+}$ ion with a distance of 5.484(2) Å. Thus, it may be a good candidate for observing the bond formation and breakage that occurs in the solid state under solvent stimuli. This is indeed the case. When the crystalline samples of complex **2** were soaked with water and immediately absorbed with filter paper, they were completely transformed into complex **1** within 1 to 2 min (Figure 5e).

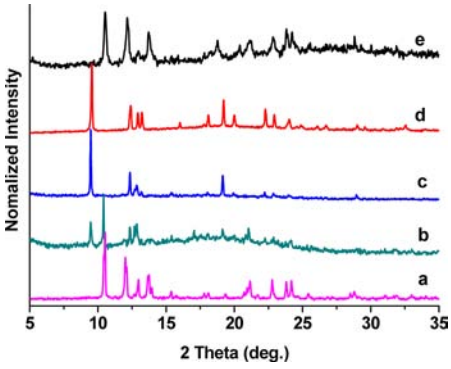


**Figure 5.** PXRD patterns of as-synthesized **1** (a), the immersion of **1** in DMF for 10 min (b) and 20 min (c), as-synthesized **2** (d), and after treatment of **2** with water for 1 to 2 min (e).

During this time course, two Eu−O (DMF) and four H···O bonds in complex **2** were broken, and two new Eu−O (aqua) and Eu−O (OBPT) bonds as well as an H···N bond in complex **1** were formed in the solid state. These drastic movements led to a structural transformation from a discrete complex to a 1D coordination polymer, which was accompanied by the transformation from a monoclinic phase ($C2/c$) to a triclinic phase ($P\bar{1}$). The successful transformation of complex **2** into complex **1** encouraged us to examine their reversibility. When complex **1** was immersed in a dried DMF solvent for 10 min, the PXRD pattern showed that a part of complex **1** was converted to complex **2** with a mixed phase (Figure 5b). However, complex **1** was completely converted to complex **2** by extending the soaking time to 20 min (Figure 5c), indicating that the transformations between complexes **1** and **2** are reversible under solvent stimuli.

To probe the transformation mechanism, the interconversion processes were monitored with a microscope. During the course of transforming **2** to **1**, the transparent crystals of **2** became opaque within 1 min when water was added. However, the shapes of the crystals were retained (Figure S9 in the Supporting Information). This was also observed for the transformation of complex **1** to complex **2** (Figure S10 in the Supporting Information). Therefore, a crystal-to-crystal transformation mechanism may be involved. To examine this mechanism further, solid−gas transformation experiments were also performed. When the microcrystalline samples of **2** were exposed to water vapor for 1 day, the PXRD pattern showed that complex **2** was completely converted to complex **1** (Figure S14 in the Supporting Information). This was also observed for the transformation of complex **1** to complex **2** by exposure to DMF vapor for 3 weeks (Figure S14 in the Supporting Information). The above experiments further prove that a dissolution and recrystallization process can be ruled out.

Furthermore, the reversible transformation between analogous complexes **3** and **4** were also examined under solvent stimuli and confirmed by PXRD measurements (Figure S5). It should be pointed out that the conversion time from complex **3** to complex **4** is 40 min in DMF solvent, which is twice that of complex **1** to complex **2**.

**Photoluminescence Properties.** When the samples were excited with a UV lamp (365 nm), complexes **1** and **2** emitted distinct colors from those of complexes **3** and **4**, as shown in Figure 6, which were readily observed with the naked eye.

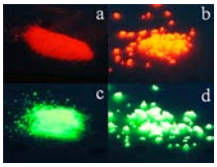


**Figure 6.** Photographs of the microcrystals of **1** (a), **2** (b), **3** (c), and **4** (d) under a UV lamp ($\lambda_{ex}$ = 365 nm). The distances from the lamp to the samples were fixed for all of the photographs.

Moreover, the photoluminescence intensity of complexes **2** and **4** is stronger than that of **1** and **3**, respectively. To look into these differences in photoluminescence properties in the solid state, excitation and emission spectra were recorded at room temperature. The excitation spectra of complexes **1** and **2** were recorded by monitoring the intensity of the $^{5}D_0 \rightarrow {}^{7}F_2$ transition of the $Eu^{3+}$ ion (615 nm for **1** and 618 nm for **2**, Figure 7). For complex **1**, a broad band that ranged from 240 to 375 nm with a peak at 335 nm can be assigned to the $\pi-\pi^*$ ligand transition, and the narrow bands that are centered at 381, 395, 416, and 465 nm can be assigned to transitions of $Eu^{3+}$ from $^{7}F_{0,1} \rightarrow {}^{5}L_7$, $^{5}L_6$, $^{5}D_3$, and $^{5}D_2$, respectively.[19] However, these transitions are weaker than the absorption of the organic ligand and are overlapped by a broad excitation band, indicating that the luminescence sensitization via the excitation of the ligand is much more efficient than the direct excitation of the $Eu^{3+}$ ion absorption level.[20] For complex **2**, the $\pi-\pi^*$ ligand transition red shifts to the range of 240−380 nm with a peak at 350 nm, which is attributed to the higher electron density of the conjugate system of the OBPT ligand in **2** resulting from the breaking of the Eu−$O_L$ bond. Meanwhile, the $^{7}F_{0,1} \rightarrow {}^{5}L_7$ transition, which is the characteristic energy level of $Eu^{3+}$ and is observed in **1**, is covered by the $\pi-\pi^*$ ligand transition in **2**, indicating that the antenna effect of the


dx.doi.org/10.1021/ic400340y | Inorg. Chem. 2013, 52, 6450−6456

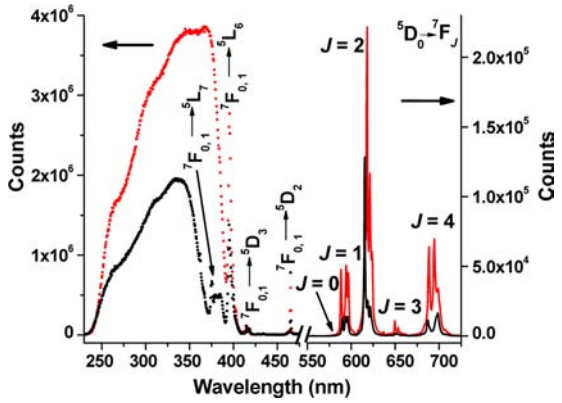


**Figure 7.** Room-temperature excitation and emission spectra for complexes **1** (black) and **2** (red) ($\lambda_{ex}$ = 350 nm).

ligand is still efficient for $Eu^{3+}$. The excitation spectra also illustrate that complex **2** is more efficiently excited than complex **1** under a UV lamp (365 nm, Figures 6 and S6). The emission spectra of **1** and **2** were recorded under the excitation wavelength at 350 nm and exhibited a classical pattern for $Eu^{3+}$ that is caused by the transition of the first excited state, $^5D_0$, to the ground septet, $^7F_J$ ($J$ = 0–4) (Figure 7).[20,21] The $^5D_0 \rightarrow {}^7F_0$ transition is very weak and is at 580 nm. The moderately strong $^5D_0 \rightarrow {}^7F_1$ transition splits into three peaks at 589, 593, and 596 nm. The peaks at about 650 and 653 nm correspond to the characteristic $^5D_0 \rightarrow {}^7F_3$ transition, and the $^5D_0 \rightarrow {}^7F_4$ transition splits into three peaks at 687, 695, and 698 nm. It is noted that the hypersensitive $^5D_0 \rightarrow {}^7F_2$ transition also splits into three peaks at 615, 618, and 621 nm, resulting in red luminescence. However, the strongest band in complex **1** is at 615 nm with a intensity ratio of $I_{615}/I_{618}$ = 5.2 that shifts to 618 nm with a ratio $I_{615}/I_{618}$ = 0.38 in complex **2**. The intensity ratio of the $I(^5D_0 \rightarrow {}^7F_2)/I(^5D_0 \rightarrow {}^7F_1)$ transitions is very sensitive to the symmetry of $Eu^{3+}$, with 9.6 for **1** and 4.5 for **2** indicating that the symmetry of the $Eu^{3+}$ site in **1** is lower than that of **2**, which is in good agreement with the results of the single-crystal X-ray analysis.

The room-temperature solid-state excitation and emission spectra of complexes **3** and **4** are presented in Figure 8. The excitation spectra of **3** and **4** were monitored around the $^5D_4 \rightarrow {}^7F_5$ transition of $Tb^{3+}$ and show broad bands in the range of 240–390 nm, which can be assigned to the $\pi$–$\pi^*$ ligand transition. The absence or weakness of the absorption bands for

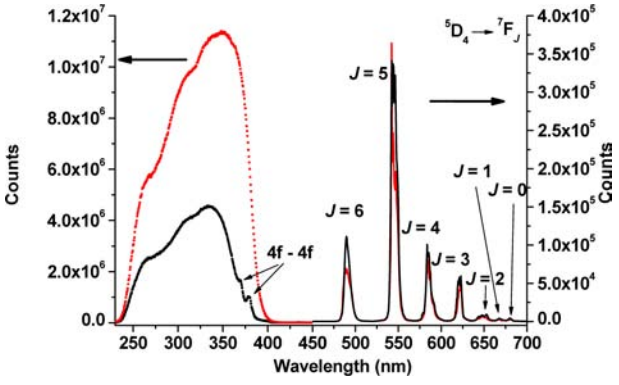


**Figure 8.** Room-temperature excitation and emission spectra for complexes **3** (black) and **4** (red) ($\lambda_{ex}$ = 350 nm).

the f–f transition of $Tb^{3+}$ indicates that the luminescence sensitization via the ligand is more sensitive. The emission spectra of **3** and **4**, excited at 350 nm, present a series of characteristic emission bands of $Tb^{3+}$ that are centered at 489, 542, 584, 623, 653, 667, and 680 nm, which result from transitions of the $^5D_4$ excited state to the corresponding ground state $^7F_J$ ($J$ = 6–0) of the $Tb^{3+}$ ion.

Room-temperature time-resolved fluorescence was carried out by monitoring the most intense emission bands of 615 nm for **1**, 618 nm for **2**, and 542 nm for **3** and **4** upon excitation, with maximum peaks of the excitation spectra at 335 nm for **1**, 370 nm for **2**, 335 nm for **3**, and 350 nm for **4**. The luminescence lifetimes of 0.54 ms for **1**, 1.40 ms for **2**, 1.00 ms for **3**, and 1.40 ms for **4** were obtained by fitting their decay curves to single-exponential functions (Figures S6 and S7 in the Supporting Information), indicating that only one emissive $Ln^{3+}$ center exists in each complex. It is worth noting that complexes **2** and **4** have longer luminescence lifetimes than those of the corresponding complexes **1** and **3**. This can be attributed to the luminescence quenching that is caused by the OH oscillators of the bonded water molecules in **1** and **3**.[19]

**Selective Sensing for Small Molecules.** The obvious enhancement of the emission intensity in **2** that is caused by the displacement of the coordinated water in **1** by DMF encouraged us to observe the solvent-induced luminescent sensing for small solvent molecules. The powdery samples of **1** were immersed in acetone, ethyl acetate (EA), ethanol, acetonitrile, methanol, THF, and DMF solvents for 0.5 h. The solvents on the surface of the samples were absorbed with filter paper, and the samples were fixed and sealed in a quartz cell for luminescence experiments upon excitation at 365 nm. The photoluminescence response of **1** for the various small molecules is shown in Figure 9. The histogram (Figure 10)

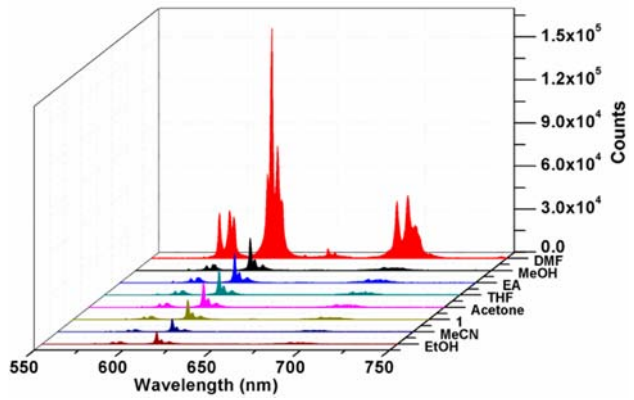


**Figure 9.** Room-temperature emission spectra of **1** upon treatment with various solvents at an excitation of 365 nm.

clearly shows that most of the solvents give a negligible change in luminescence; however, DMF triggers a marked luminescence enhancement of more than 11-fold. Moreover, the strongest band is shifted from 615 to 618 nm.

To gain structural insights into the enhancement of luminescence with respect to the selectivity of the DMF molecule, PXRD of the solvent-treated samples was carried out and compared to that of **1**. As shown in Figure 11, the PXRD patterns of the samples that were immersed in acetone, EA, ethanol, acetonitrile, methanol, and THF solvents were almost the same as that of **1**. However, the pattern of the DMF-treated


dx.doi.org/10.1021/ic400340y | Inorg. Chem. 2013, 52, 6450–6456

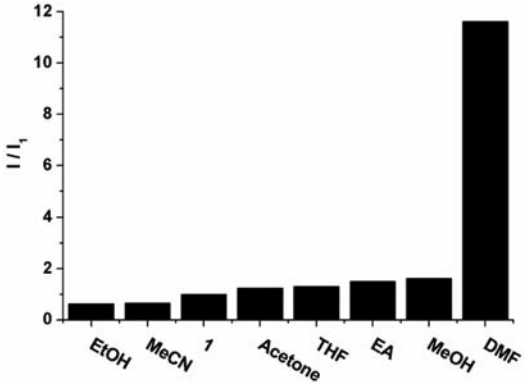


**Figure 10.** Diagram of the peak intensity ratio of $^5D_0 \rightarrow {}^7F_2$ vs solvent upon excitation at 365 nm.

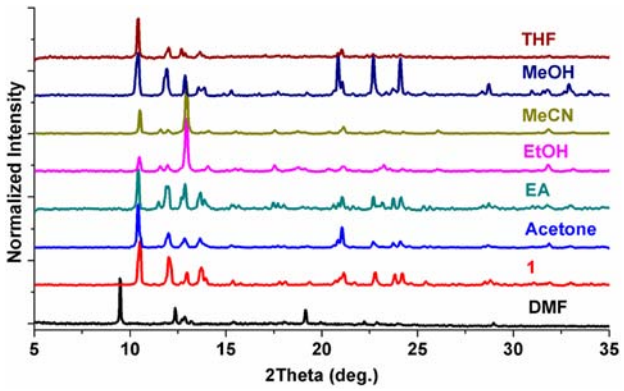


**Figure 11.** Powder X-ray diffraction patterns of complex **1** by immersing its powdery sample in the indicated solvents for 0.5 h.

sample was significantly changed and matched well with that of **2** (Figure 5), indicating that **1** is transformed to **2** under DMF treatment. This is consistent with the aforementioned observations of the crystal-to-crystal transformation.

As described above, the coordinated water in **1** is displaced by DMF molecules, leading to a structural conversion from a 1D coordination polymer to discrete complex **2** and the marked enhancement of its emission intensity. However, a negligible change in emission spectra for other ordinary solvents, such as acetone, EA, ethanol, acetonitrile, methanol, and THF, was observed, indicating that **1** is a potential sensing material for DMF molecules with a high selectivity. Furthermore, complex **3** also shows a selective luminescence enhancement (3.5 times) in response to DMF when compared to that observed for the other examined solvents (Figures S11 and S12 in the Supporting Information). It is worth mentioning that a few sensing materials for small molecules have been reported and most of them involve the adsorption and desorption of the small molecules.[22]

## CONCLUSIONS

Two solvent-mediated 1D coordination polymers and two discrete complexes have been synthesized. The reversible crystal-to-crystal transformations between them were achieved by immersing the crystalline samples into the corresponding solvents or exposing them to solvent vapor. Complex **1** shows a highly selective luminescence enhancement in response to DMF when compared to that observed for the other examined solvents. Structure and luminescence lifetime studies suggest that the majority of the luminescence enhancement in response to DMF is caused by the displacement of the aqua ligand by DMF molecules.

## ASSOCIATED CONTENT

### Supporting Information

Deposition nos. CCDC 914 943 and 914 944 contain the supplementary crystallographic data for complexes **1** and **2**, respectively. These data can be obtained free of charge from The Cambridge Crystallographic Data Centre via www.ccdc.cam.ac.uk/data_request/cif. TGA for complexes **1** and **3**, PXRD patterns for **1**−**4**, crystal-to-crystal transformation between **3** and **4**, decay curves and corresponding fitting curves for **1**−**4**, selected bond distances and angles for **1** and **2**, photographs for crystal-to-crystal transformation between **1** and **2**, PXRD patterns for the solid−gas transformation, and luminescence changes in complex **3** sensing for solvents. This material is available free of charge via the Internet at http://pubs.acs.org.

## AUTHOR INFORMATION

### Corresponding Author

*E-mail: caoml@mail3.sysu.edu.cn (M.L.C.), cesybh@mail.sysu.edu.cn (B.H.Y.).

### Notes

The authors declare no competing financial interest.

## ACKNOWLEDGMENTS

This work was supported by the NSF of China (21 071 154, 21 001 031, 21 272 284, and J1 103 305) and the DPF of MOE of China (0 171 110 04). We thank Mr. De-Jian Hou for helpful discussions.

## REFERENCES

(1) Macgillivray, L. R.; Papaefstathiou, G. S.; Friscic, T.; Hamilton, T. D.; Bucar, D. K.; Chu, Q.; Varshney, D. B.; Georgiev, I. G. *Acc. Chem. Res.* **2008**, *41*, 280.

(2) (a) Kitagawa, S.; Matsuda, R. *Coord. Chem. Rev.* **2007**, *251*, 2490. (b) Kawano, M.; Fujita, M. *Coord. Chem. Rev.* **2007**, *251*, 2592. (c) Vittal, J. J. *Coord. Chem. Rev.* **2007**, *251*, 1781. (d) Kole, G. K.; Vittal, J. J. *Chem. Soc. Rev.* **2013**, *42*, 1755.

(3) (a) Zhang, J.-P.; Lin, Y.-Y.; Zhang, W.-X.; Chen, X.-M. *J. Am. Chem. Soc.* **2005**, *127*, 14162. (b) Mobin, S. M.; Srivastava, A. K.; Mathur, P.; Lahiri, G. K. *Dalton Trans.* **2010**, *39*, 8698. (c) Sarma, D.; Natarajan, S. *Cryst. Growth Des.* **2011**, *11*, 5415. (d) Fang, Z.-L.; Yu, R.-M.; Wu, X.-Y.; Huang, J.-S.; Lu, C.-Z. *Cryst. Growth Des.* **2011**, *11*, 2546. (e) Coronado, E.; Giménez-Marqués, M.; Espallargas, G. M. *Inorg. Chem.* **2012**, *51*, 4403. (f) Wang, X.-F.; Wang, Y.; Zhang, Y.-B.; Xue, W.; Zhang, J.-P.; Chen, X.-M. *Chem. Commun.* **2012**, *48*, 133.

(4) (a) Mir, M. H.; Koh, L. L.; Tan, G. K.; Vittal, J. J. *Angew. Chem., Int. Ed.* **2010**, *49*, 390. (b) Georgiev, I. G.; Bučar, D.-K.; MacGillivary, L. R. *Chem. Commun.* **2010**, *46*, 4956. (c) Liu, D.; Li, N.-Y.; Lang, J.-P. *Dalton Trans.* **2011**, *40*, 2170. (d) Yu, W.-B.; Han, Y.-F.; Lin, Y.-J.; Jin, G.-X. *Chem.—Eur. J.* **2011**, *17*, 1863. (e) Xie, M.-H.; Yang, X.-L.; Wu, C.-D. *Chem.—Eur. J.* **2011**, *17*, 11424. (f) Ou, Y.-C.; Zhi, D.-S.; Liu, W.-T.; Ni, Z.-P.; Tong, M.-L. *Chem.—Eur. J.* **2012**, *18*, 7537. (g) Sato, H.; Matsuda, R.; Mir, M. H.; Kitagawa, S. *Chem. Commun.* **2012**, *48*, 7919.

(5) (a) Ghosh, S. K.; Kaneko, W.; Kiriya, D.; Ohba, M.; Kitagawa, S. *Angew. Chem., Int. Ed.* **2008**, *47*, 8843. (b) Férey, G.; Serre, C. *Chem. Soc. Rev.* **2009**, *38*, 1380. (c) Duan, Z.; Zhang, Y.; Zhang, B.; Zhu, D. *CrystEngComm* **2011**, *13*, 6801. (d) Liu, Z.-Y.; Yang, E.-C.; Li, L.-L.; Zhao, X.-J. *Dalton Trans.* **2012**, *41*, 6827. (e) Bloch, W. M.; Sumby, C. J. *Chem. Commun.* **2012**, *48*, 2534. (f) Li, H.; Wang, X.; Jia, Y.; Zhao, B.; Ding, R.; Huo, H. W.; Fan, Y. *CrystEngComm* **2012**, *14*, 5155.

(6) Sun, J.; Dai, F.; Yuan, W.; Bi, W.; Zhao, X.; Sun, W.; Sun, D. *Angew. Chem., Int. Ed.* **2011**, *50*, 7061.
(7) Cui, X.; Khlobystov, A. N.; Chen, X.; Marsh, D. H.; Blake, A. J.; Lewis, W.; Champness, N. R.; Roberts, C. J.; Schröder, M. *Chem.—Eur. J.* **2009**, *15*, 8861.
(8) (a) Lv, G.-C.; Wang, P.; Liu, Q.; Fan, J.; Chen, K.; Sun, W.-Y. *Chem. Commun.* **2012**, *48*, 10249. (b) Adarsh, N. N.; Grelard, A.; Dufourc, E. J.; Dastidar, P. *Cryst. Growth Des.* **2012**, *12*, 3369. (c) Manos, M. J.; Kyprianidou, E. J.; Papaefstathiou, G. S.; Tasiopoulos, A. J. *Inorg. Chem.* **2012**, *51*, 6308. (d) He, Y.-C.; Yang, J.; Yang, G.-C.; Kan, W.-Q.; Ma, J.-F. *Chem. Commun.* **2012**, *48*, 7859. (e) Song, Y.-M.; Luo, F.; Luo, M.-B.; Liao, Z.-W.; Sun, G.-M.; Tian, X.-Z.; Zhu, Y.; Yuan, Z.-J.; Liu, S.-J.; Xu, W.-Y.; Feng, X.-F. *Chem. Commun.* **2012**, *48*, 1006. (f) Wang, Q.-L.; Southerland, H.; Li, J.-R.; Prosvirin, A. V.; Zhao, H.; Dunbar, K. R. *Angew. Chem., Int. Ed.* **2012**, *51*, 9321.
(9) (a) Cheng, K.; Foxman, B. M. *J. Am. Chem. Soc.* **1977**, *99*, 8102. (b) Cheng, X.-N.; Zhang, W.-X.; Chen, X.-M. *J. Am. Chem. Soc.* **2007**, *129*, 15738. (c) Heo, J.; Jeon, Y.-M.; Mirkin, C. A. *J. Am. Chem. Soc.* **2007**, *129*, 7712. (d) Adams, C. J.; Colquhoun, H. M.; Crawford, P. C.; Lusi, M.; Orpen, A. G. *Angew. Chem., Int. Ed.* **2007**, *46*, 1124. (e) Katz, M. J.; Ramnial, T.; Yu, H.-Z.; Leznoff, D. B. *J. Am. Chem. Soc.* **2008**, *130*, 10662. (f) Peedikakkal, A. M. P.; Koh, L. L.; Vittal, J. J. *Chem. Commun.* **2008**, 441. (g) Liu, D.; Li, M.; Li, D. *Chem. Commun.* **2009**, 6943. (h) Zhang, Y.-J.; Liu, T.; Kanegawa, S.; Sato, O. *J. Am. Chem. Soc.* **2009**, *131*, 7942. (i) Kondo, A.; Nakagawa, T.; Kajiro, H.; Chinen, A.; Hattori, Y.; Okino, F.; Ohba, T.; Kaneko, K.; Kanoh, H. *Inorg. Chem.* **2010**, *49*, 9247. (j) Gheorghe, R.; Kalisz, M.; Clerac, R.; Mathoniere, C.; Herson, P.; Li, Y.; Seuleiman, M.; Lescouezec, R.; Lloret, F.; Julve, M. *Inorg. Chem.* **2010**, *49*, 11045. (k) Zhang, B.; Zhu, D.; Zhang, Y. *Chem.—Eur. J.* **2010**, *16*, 9994. (l) Liu, T.-F.; Chen, Y.-P.; Yakovenko, A. A.; Zhou, H.-C. *J. Am. Chem. Soc.* **2012**, *134*, 17358. (m) Lassig, D.; Lincke, J.; Gerhardt, R.; Krautscheid, H. *Inorg. Chem.* **2012**, *51*, 6180.
(10) (a) Chen, B.; Wang, L.; Zapata, F.; Qian, G.; Lobkovsky, E. B. *J. Am. Chem. Soc.* **2008**, *130*, 6718. (b) Lan, Y.-Q.; Jiang, H.-L.; Li, S.-L.; Xu, Q. *Inorg. Chem.* **2012**, *51*, 7484.
(11) (a) Cao, M.-L.; Hao, H.-G.; Zhang, W.-X.; Ye, B.-H. *Inorg. Chem.* **2008**, *47*, 8126. (b) Cao, M.-L.; Hao, H.-G.; Ye, B.-H. *Cryst. Growth Des.* **2009**, *9*, 546. (c) Cao, M.-L.; Wu, J.-J.; Mo, H.-J.; Ye, B.-H. *J. Am. Chem. Soc.* **2009**, *131*, 3458.
(12) Cao, M.-L. *Acta Crystallogr., Sect. E: Struct. Rep.* **2011**, *67*, M739.
(13) Wu, J.-J.; Xue, W.; Cao, M.-L.; Qiao, Z.-P.; Ye, B.-H. *CrystEngComm* **2011**, *13*, 5495.
(14) Wu, J.-J.; Cao, M.-L.; Zhang, J.-Y.; Ye, B.-H. *RSC Adv.* **2012**, *2*, 12718.
(15) (a) Cao, M.-L.; Zhang, X.-L.; Yin, W. *Chin. J. Inorg. Chem.* **2011**, *27*, 1635. (b) Cao, M.-L.; Zhang, X.-L.; Yin, W. *Chin. J. Struct. Chem.* **2012**, *31*, 499.
(16) Blessing, R. H. *Acta Crystallogr., Sect. A* **1995**, *51*, 33.
(17) Sheldrick, G. M. *SHELXS-97, a Program for Crystal Structure Solution*; Göttingen University: Göttingen, Germany, 1997.
(18) Sheldrick, G. M. *SHELXL-97, a Program for Crystal Structure Refinement*; Göttingen University: Göttingen, Germany, 1997.
(19) (a) Horrocks, W. D., Jr.; Sudnick, D. R. *J. Am. Chem. Soc.* **1979**, *101*, 334. (b) Eliseeva, S. V.; Bünzli, J.-C. G. *Chem. Soc. Rev.* **2010**, *39*, 189.
(20) (a) Ramya, A. R.; Sharma, D.; Natarajan, S.; Reddy, M. L. P. *Inorg. Chem.* **2012**, *51*, 8818. (b) Reddy, M. L. P.; Sivakumar, S. *Dalton Trans.* **2013**, *42*, 2663.
(21) (a) Gai, Y.-L.; Xiong, K.-C.; Chen, L.; Bu, Y.; Li, X.-J.; Jiang, F.-L.; Hong, M.-C. *Inorg. Chem.* **2012**, *51*, 13128. (b) Li, Y.-A.; Ren, S.-K.; Liu, Q.-K.; Ma, J.-P.; Chen, X.; Zhu, H.; Dong, Y.-B. *Inorg. Chem.* **2012**, *51*, 9629. (c) Zhan, C.-H.; Wang, F.; Kang, Y.; Zhang, J. *Inorg. Chem.* **2012**, *51*, 523.
(22) (a) Chen, B.; Yang, Y.; Zapata, F.; Lin, G.; Qian, G.; Lobkovsky, E. B. *Adv. Mater.* **2007**, *19*, 1693. (b) Xiao, Y.; Cui, Y.; Zheng, Q.; Xiang, S.; Qian, G.; Chen, B. *Chem. Commun.* **2010**, *46*, 5503. (c) Chen, B.; Wang, L.; Xiao, Y.; Fronczek, F. R.; Xue, M.; Cui, Y.; Qian, G. *Angew. Chem., Int. Ed.* **2009**, *48*, 500. (d) Lu, W.-G.; Jiang, L.; Feng, X.-L.; Lu, T.-B. *Inorg. Chem.* **2009**, *48*, 6997. (e) Lu, Z.-Z.; Zhang, R.; Li, Y.-Z.; Guo, Z.-J.; Zheng, H.-G. *J. Am. Chem. Soc.* **2011**, *133*, 4172. (f) Lan, A.; Li, K.; Wu, H.; Olson, D. H.; Emge, T. J.; Ki, W.; Hong, M.; Li, J. *Angew. Chem., Int. Ed.* **2009**, *48*, 2334. (g) Lu, G.; Hupp, J. T. *J. Am. Chem. Soc.* **2010**, *132*, 7832. (h) Guo, Z.; Xu, H.; Su, S.; Cai, J.; Dang, S.; Xiang, S.; Qian, G.; Zhang, H.; O'Keeffe, M.; Chen, B. *Chem. Commun.* **2011**, *47*, 5551. (i) Gole, B.; Bar, A. K.; Mukherjee, P. S. *Chem. Commun.* **2011**, *47*, 12137. (j) Li, Y.; Zhang, S.; Song, D. *Angew. Chem., Int. Ed.* **2013**, *52*, 710.